

A multi-scale “morphological approach” for highly-filled particulate composites: evaluation in hyperelasticity and first application to viscohyperelasticity

M. TOUBOUL¹), C. NADOT–MARTIN¹), A. DRAGON¹),
A. FANGET²)

¹) *Laboratoire de Mécanique de Physique des Matériaux (UMR CNRS 6617)
Téléport 2, 1 av. Clément Ader, BP 40109
86961 Futuroscope-Chasseneuil Cedex, France*

²) *Centre d'Etudes de Gramat
46500 Gramat, France*

THIS ARTICLE DEALS with a non-classical scale transition devoted, in the long-run, to the prediction of the nonlinear mechanical behavior of energetic composites. A geometrical and kinematical schematization of the microstructure is defined as a conspicuous starting point for further localization-homogenization procedure. Thus, salient information on the morphology and some intraphase heterogeneity are taken into account. The first results obtained in a finite strain context for a three-dimensional periodic microstructure are compared to the finite element solution. Furthermore, the ability of the methodology to deal with viscohyperelasticity in a direct manner is illustrated. This is a significant step towards efficient mastery of the scale transition for viscoelastic aggregates, whose inherent characteristic lies in space/time local interactions and relative “long-memory” effect.

1. Introduction

THIS STUDY is part of a long-time research program aiming at predicting the vulnerability of energetic composites, i.e. highly filled particulate composites such as propellant-like materials. To this end, a multi-scale modeling able not only to characterize the macroscopic behavior of the composite by taking into account structural morphology, but also to provide estimates of local fields had to be developed. Moreover, the methodology concerned should be adapted to the random microstructures of the materials studied, characterized notably by a high proportion (>60% in volume) of irregular grains. A non-classical approach, seeming suitable for the purpose, has been advanced in 1983 by CHRISTOFFERSEN [1] in small strain linear elasticity. Some of the present authors have developed it further outside this range in order to embrace first the dissipative

effects and second – the finite deformation context. So, it has been first applied and extended in small strain viscoelasticity (see NADOT–MARTIN *et al.* [2]). Viscoelastic behavior is a strong challenge indeed for any credible scale transition approach as it involves accounting for truly space/time marked interactions of constituents on the local level and next their macroscopic consequences, notably the remarkable “long-range memory effect”, see for example [2] and BEURTHEY and ZAOUI [3]. The latter states, at elementary level, that global behavior of an aggregate of, say, Maxwellian viscoelastic constituents, is all but Maxwellian viscoelasticity; the non-Maxwellian contribution signifying the “long-memory” term, see for example SUQUET [4].

In order to match progressively applications at stake for highly filled elastomers, the Christoffersen-type approach has then been reset to finite strain (see GUIOT *et al.* [5]). The specificity of the approach lies notably in a direct geometrical schematization of the real microstructure, defined and treated upstream, i.e. before proceeding with the scale transition itself. Some rich and relevant information concerning morphology and internal arrangement of the constituents is taken into account explicitly in the local and global estimates, via the geometrical parameters defined during this first schematizing step. This constitutes an important feature knowing that a fair description of a representative volume element (R.V.E.) has always been a key issue in the context of “averaging methods” [6]. For random microstructures, only partial information is available. Commonly, some statistical information is accounted for using correlation functions, i.e. mathematical tools that may be hardly measurable and usable. This led BORNERT [7] to propose the concept of a “morphologically representative pattern”, supposed to be more representative of the real morphology. The specific geometrical schematization dealt with here responds to the willingness to take into account accurate and relevant morphological information for a particular class of heterogeneous materials, namely, the particulate composites. Moreover, the coupling between this morphological insight and a local kinematics postulated (assumptions regarding notably the matrix-related displacement field) offers a way to take into account some intraphase heterogeneity in the homogenized behavior estimate. Thus, the morphology-based approach advanced faces another current major challenge in nonlinear micromechanics: the introduction of field fluctuation indicators in order to improve the description of local heterogeneity whose important effect on the nonlinear macroscopic behavior has been shown (see for example MOULINEC and SUQUET [8], PONTE–CASTAÑEDA [9, 10], IDIART *et al.* [11, 12]).

The objectives here are to present the first quantitative evaluation of the transformed Christoffersen-type method (which will be denoted further as the “morphological approach”) in the finite strain framework, and then to illustrate its possible applicability in the context of viscohyperelasticity which is an es-

sential feature of the energetic composites. To this end, in Sec. 2, the main ingredients of the morphological approach reset to finite strain by GUIOT *et al.* [5] are recalled and discussed. Next, the relevance of estimates obtained by this means is evaluated in the simplified context of a three-dimensional composite with hyperelastic constituents and periodic microstructure (Sec. 3). The foregoing “model” microstructure is subjected to various loading paths (uniaxial compressive deformation, incompressible tension and simple shear). Global as well as local estimates are compared with the results given by the finite element method. This kind of comparison (using numerical tools such as finite elements, or Fast Fourier Transform [13]) is indeed commonly admitted today as a possible accuracy standard regarding micromechanics methods’ applicability and reliability, see for example [12, 14]. Finally, Sec. 4 aims at proving the ability of the method to deal with viscohyperelasticity in a direct manner. Current challenges mentioned above in the framework of time-dependent behavior of heterogeneous media are first recalled. Then, the constitutive model describing the viscohyperelasticity of the matrix is presented (Sec. 4.1) and the particular algorithm developed to solve the localization-homogenization problem in the general case of random microstructure is detailed (Sec. 4.2). The latter section ends by illustrating the qualitative relevance of the first results obtained for the periodic microstructure considered in Sec. 3.

2. Christoffersen-type approach in the finite strain framework

In this section, the generalization to finite strain of CHRISTOFFERSEN’s original approach [1] is given in a Lagrangian framework. The main features of this methodology (see also Sec. 2 in GUIOT *et al.* [5]) are presented and discussed.

2.1. Geometrical and kinematical schematizations

The approach starts with a geometrical schematization of initial random microstructure of the considered material. In the initial configuration, the grains of a highly filled particulate composite are represented by polyhedra; the matrix phase is discretized by an assembly of thin layers with constant thicknesses separating the polyhedral grains. This schematization is illustrated in Fig. 1 (two-dimensional representation). For each layer α , a set of four “morphological parameters” is defined in the non-deformed configuration:

- h^α , the constant thickness of layer α ;
- A^α , the projected area of layer α ; the associated volume is then $A^\alpha h^\alpha$;
- \mathbf{d}^α , the vector linking the centroids of the two polyhedra (grains) separated by layer α ;
- \mathbf{n}^α , the unit vector normal to the plane interface grain/layer α .

Once the grains are replaced by polyhedra (satisfying the condition of parallelism between the interfaces of opposite grains), the parameters \mathbf{d}^α , \mathbf{n}^α and h^α are readily determined. For a random microstructure, the projected area A^α – leading to the definition of the matrix zone between two neighboring grains called “layer α ” – may be determined as follows. Starting from the centroids of the two considered grains, the two opposite interfaces are projected on the middle plane of the intergranular zone. Then, an average projection is defined and chosen as the area A^α . In this way, layer α (associated volume $A^\alpha h^\alpha$) does not correspond exactly to the matrix zone strictly confined between the two opposite interfaces. It can be larger as illustrated in Fig. 1.

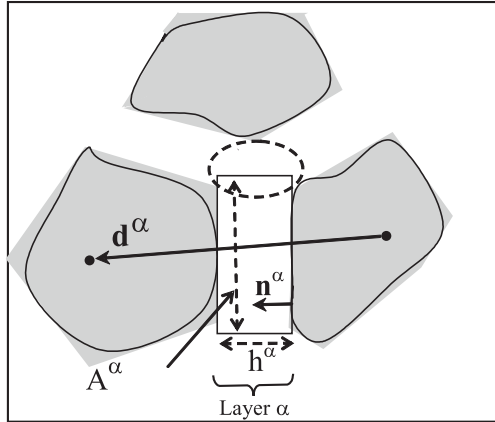


FIG. 1. Microstructure geometrical schematization (two-dimensional illustration) by CHRISTOFFERSEN [1].

Even if such a geometrical schematization (polyhedral grains, parallelism of opposite interfaces) is an approximation of the particulate microstructure, salient information concerning real morphology is nevertheless accounted for in the considered approach. In the original paper of CHRISTOFFERSEN [1], dependence of estimates on possible texture of the considered composite, on grain shapes' irregularities and on layers' thicknesses is demonstrated; in finite strain, this is obviously preserved. From the practical point of view, the challenge is to optimize the correspondence of the “true” microstructure with the Christoffersen-schematized one, in order to confer a fair relevance on the morphological parameters involved in the estimates.

The second step of the approach is the formulation of simplifying kinematical assumptions concerning the local fields in the schematized volume. They are recalled below and are the direct generalization to finite strain of the Christoffersen's original kinematical hypotheses:

- the deformation gradient in the grains, denoted \mathbf{f}^0 , is supposed to equal the macroscopic deformation gradient \mathbf{F} at the centroids of the grains; \mathbf{F} is considered as the data of the localization-homogenization problem;
- \mathbf{f}^0 is assumed to be homogeneous and identical for all the grains;
- the deformation gradient in a layer, denoted \mathbf{f}^α , is supposed to be homogeneous in that layer, but it can vary from one layer to another;
- local disturbances at grain edges and corners (see circled zone in Fig. 1) are neglected on the basis of thinness of the layers.

2.2. Local problem approach

In this doubly schematized context (morphological and kinematical), using the continuity of displacements at the interfaces between the grains and layers, the deformation gradient \mathbf{f}^α of any layer α can be expressed as a function of the morphological parameters proper to this layer:

$$(2.1) \quad f_{iJ}^\alpha = f_{iJ}^0 + (F - f^0)_{iK} \frac{d_K^\alpha n_J^\alpha}{h^\alpha}.$$

As a consequence, the deformation gradient in layer χ will be different from the one in layer α (since its morphological parameters are different from the ones of layer α). Thus, Christoffersen’s morphology and kinematics framework extended to finite strain offers a way to take into account some strain heterogeneity in the matrix phase represented by an assembly of layers. This constitutes a positive feature in the context of nonlinear homogenization as it has been shown that local heterogeneity has to be taken into account to ensure a fair estimate of the macroscopic behavior of a nonlinear heterogeneous body (see in the finite strain framework the work by LOPEZ-PAMIES and PONTE-CASTAÑEDA [15] for an application of the improved second-order theory, incorporating field fluctuations [9] to hyperelastic composites).

On the contrary, the hypothesis of identical deformation gradient \mathbf{f}^0 for all grains (allowing no heterogeneity in the grain phase) could seem somewhat reductive. However, it remains reasonable for highly-filled particulate composites where the matrix is much softer than the grains, and where it is the matrix that accommodates much of the strain, keeping in mind that the deformation gradient in the matrix phase varies from one layer to another.

The compatibility between local motion defined in the above schematized context (see Subsec. 2.1) and the macroscopic one, characterized by the given deformation gradient \mathbf{F} , is ensured through the following equation:

$$(2.2) \quad \mathbf{F} = \langle \mathbf{f} \rangle_{V_0} = (1 - c) \mathbf{f}^0 + \frac{1}{V_0} \sum_{\alpha} \mathbf{f}^\alpha A^\alpha h^\alpha$$

which is valid only if the following “compatibility condition” (2.3) is satisfied:

$$(2.3) \quad \frac{1}{V_0} \sum_{\alpha} d_I^{\alpha} n_J^{\alpha} A^{\alpha} = \delta_{IJ}.$$

In (2.2) and (2.3) V_0 denotes the volume occupied by the polyhedra-and-layers assembly, c is the layers’ concentration with respect to volume V_0 ($c = \frac{1}{V_0} \sum_{\alpha} A^{\alpha} h^{\alpha}$) and δ_{IJ} is the Kronecker symbol. From a practical viewpoint, the Eq. (2.3) has to be satisfied by the parameters of the schematized microstructure in order to ensure the compatibility between local and global motions in the sense of Eq. (2.2). Involving both the size of the volume V_0 and the morphology of the schematized microstructure (and consequently, the one of the real material), Eq. (2.3) has to be considered as a double criterion. It has to be taken into account to determine the size of the mechanical representative volume element (R.V.E.) associated with the methodology at stake, and then to conclude on the applicability of the approach itself for a given material.

Using the Hill–Mandel principle of macro-homogeneity –generalized to finite strain in the case of homogeneous stress boundary conditions and applied in the context considered – the following system (2.4) is obtained:

$$(2.4) \quad \begin{aligned} \bar{S}_{Ji} &= \langle \bar{s}_{Ji} \rangle_{V_0} = (1 - c) \bar{s}_{Ji}^0 + \frac{1}{V_0} \sum_{\alpha} \bar{s}_{Ji}^{\alpha} A^{\alpha} h^{\alpha}, \\ \bar{S}_{Ji} &= \frac{1}{V_0} \sum_{\alpha} t_i^{\alpha} d_J^{\alpha}; \quad t_i^{\alpha} = \bar{s}_{Ii}^{\alpha} n_I^{\alpha} A^{\alpha}. \end{aligned}$$

$\bar{\mathbf{S}}$, $\bar{\mathbf{s}}^0$ and $\bar{\mathbf{s}}^{\alpha}$ denote the average nominal stress tensors, respectively macroscopic and microscopic in the grains and in layer α . Note that, although the first averaging is “classically” exploited, the second one remains specific to the Christoffersen-type approach: stresses are seen from a granular viewpoint as forces transmitted from grain to grain by layers acting as contact zones.

According to the Christoffersen original methodology, the local constitutive laws are introduced at this stage in order to obtain next the local problem solution by determination of the grain deformation gradient \mathbf{f}^0 . Indeed, the latter is searched in such a way that the estimated stress field, associated to the strain field by the local constitutive laws, satisfies the system (2.4), i.e. the relationship as follows:

$$(2.5) \quad (1 - c) \bar{s}_{Ji}^0 + \frac{1}{V_0} \sum_{\alpha} \bar{s}_{Ji}^{\alpha} A^{\alpha} h^{\alpha} - \frac{1}{V_0} \sum_{\alpha} \bar{s}_{Ki}^{\alpha} n_K^{\alpha} A^{\alpha} d_J^{\alpha} = 0.$$

The practical methodology of the solution of the local problem is as follows. In (2.5), the local constitutive laws concerning the grain and matrix phases allow to express

(i) $\bar{\mathbf{s}}^0$ in function of \mathbf{f}^0 ,

(ii) $\bar{\mathbf{s}}^\alpha$ for each layer α as a function of \mathbf{f}^0 and \mathbf{F} , the macroscopic deformation gradient for $\bar{\mathbf{s}}^0$ the grain constitutive law is sufficient whereas.

For $\bar{\mathbf{s}}^\alpha$ the relation (2.1) is required in addition to the matrix constitutive law. By doing so, Eq. (2.5) involves now macroscopic deformation gradient \mathbf{F} , the local morphological parameters characterizing the whole set of layers and \mathbf{f}^0 , the unknown quantity to be determined. It is then numerically solved by considering \mathbf{F} as the data for the localization-homogenization problem characterizing the loading applied. The knowledge of \mathbf{f}^0 allows the backwards calculation of the composite response at both scales. For example, for any layer α , the deformation gradient \mathbf{f}^α is given by Eq. (2.1). The corresponding stress tensor is then accessible, knowing \mathbf{f}^α and the constitutive law for the matrix. At last, the macroscopic nominal stress tensor $\bar{\mathbf{S}}$ is calculated by averaging over the local field according to (2.4)₁.

It should be noted that the homogeneous stress boundary conditions are used only in a theoretical manner for establishment of the system (2.4) using the Hill–Mandel principle of macro-homogeneity; in practice, the loading is applied via the given macroscopic deformation gradient \mathbf{F} with respect to the original Christoffersen theory. One may prove that the solution of the localization-homogenization problem obtained for a given loading path represented by \mathbf{F} according to such a strategy, satisfies (2.2) under the morphological condition (2.3), and the relation $\mathbf{S}:\mathbf{F} = \langle \bar{\mathbf{s}} : \mathbf{f} \rangle_{V_0}$ where $\bar{\mathbf{S}}$ is calculated by $\bar{\mathbf{S}} = \langle \bar{\mathbf{s}} \rangle_{V_0}$.

At last, one may emphasize that the knowledge of the local deformation gradients \mathbf{f}^0 and \mathbf{f}^α allows to calculate both the pure strain and rotation in grains and layers by using the polar decomposition. Furthermore, one could access to any measures of strain and stress in the constituents. This is another essential advantage to be pointed out in addition to the relative simplicity of the above detailed solving procedure.

3. Evaluation involving hyperelastic behavior of constituents

The previous approach being applied to a real material, the difference between experimental curves and numerical ones will be due to three error sources: the description of constituents’ behavior, the geometrical schematization and the kinematical one. The two last factors are proper to the approach exposed in Sec. 2 and have to be quantified in order to conclude on the performance of the method. Furthermore, the simplifying kinematical assumptions have to be checked first in a geometrically nonlinear context. This section constitutes an essential preliminary stage towards this aim. This is done by making comparisons between finite element (F.E.) results (using Abaqus[®]) and estimates given by

the morphological approach (M.A.) (using Mathematica[®]), considering a particular microstructure and using the same constitutive laws in both methods to describe the constituents' hyperelasticity.

3.1. Material geometry and relative representations

A three-dimensional composite with periodic microstructure is considered in orthonormal basis ($\mathbf{e}^1, \mathbf{e}^2, \mathbf{e}^3$). It is constituted of cubic grains (size: 0.2mm) regularly arranged in the matrix occupying 25 per cent of the volume as shown in Fig. 2 (distance between two grains: 0.02mm). This microstructure has been chosen for three reasons. At first, the requirements of the geometrical pattern proposed by Christoffersen are respected (polyhedral grains, plane and parallel opposite interfaces, thin layers). Consequently, only the effects of the kinematical hypotheses will be evaluated. Secondly, thanks to the periodicity of the microstructure, F.E. calculations to be performed on a unit cell can be done easily in the three-dimensional case. On the contrary, for a random microstructure, the question of the size of the R.V.E. and the one of CPU time – for nonlinear context at stake – would arise. At last, analysis of local response is simplified because of microstructure simple geometry, which is important for a first quantitative evaluation.

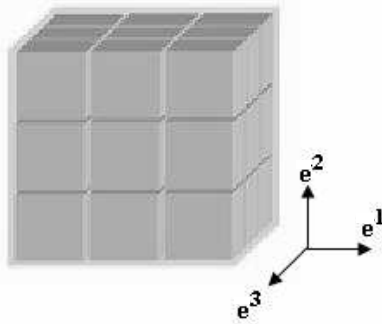


FIG. 2. Three-dimensional periodic microstructure studied.

Regarding the F.E. modeling, the unit cell considered is composed of one cubic grain (size $T_g = 0.2$ mm) embedded in a hollow cube of matrix (thickness = 0.01 mm = half of the intergranular distance). As shown in Fig. 3, the grain is meshed with 1000 identical hybrid cubic elements (C3D8H in Abaqus[®]) and the matrix with 21184 identical elements of the same type. The latter has been finely meshed because it is more compliant than the grain (as already mentioned at the beginning of Sec. 2.2); it will then accommodate most of the deformation. Furthermore, effects such as local heterogeneity will probably concentrate in this phase.

REMARK 1. More calculations have been performed using a finer mesh (in the grain and in the matrix phase); similar results were obtained.

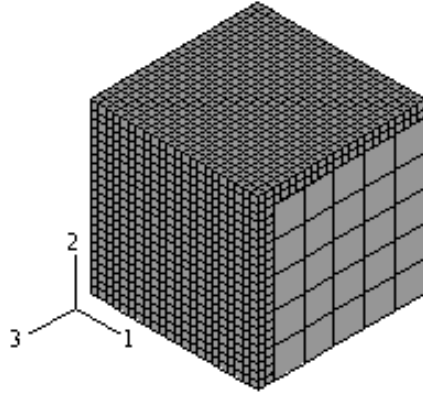


FIG. 3. Eighth of the unit cell regarding the finite element modeling.

In the morphological approach (M.A.), both the volume V_0 concerned, for which Equation (2.5) will be solved, and the morphological parameters characterizing the layers (defined in Sec. 2.1) have to be defined. As previously mentioned, the microstructure considered conforms with the geometrical schematization's requirements. Because of the periodicity of the microstructure, it is sufficient to consider only one grain (size $T_g = 0.2$ mm) together with three layers: “layer 1” whose normal unit vector \mathbf{n}^1 is \mathbf{e}^1 , “layer 2” whose normal unit vector \mathbf{n}^2 is \mathbf{e}^2 and “layer 3” whose normal unit vector \mathbf{n}^3 is \mathbf{e}^3 . The distance between two grains being the same in the three directions \mathbf{e}^1 , \mathbf{e}^2 and \mathbf{e}^3 , the three layers naturally have:

- the same thickness $h = 0.02$ mm,
- vectors \mathbf{d} with the same norm $d = \|\mathbf{d}\| = T_g + h = 0.22$ mm but different orientations: $\mathbf{d}^1 = d \mathbf{e}^1$, $\mathbf{d}^2 = d \mathbf{e}^2$ and $\mathbf{d}^3 = d \mathbf{e}^3$,
- the same projected area A .

In this particular case, the projected area A , defining the volume Ah of each layer, can be calculated so that the “compatibility condition” (2.3) is exactly satisfied, i.e. so that the compatibility between local and global motions will be ensured by Eq. (2.2). Indeed, for $I \neq J$ equality $\frac{1}{V_0} \sum_{\alpha=1}^3 d_I^\alpha n_J^\alpha A = 0$ is satisfied (because of the orientations of \mathbf{d}^α and \mathbf{n}^α) and for $I = J$, one obtains the following condition to be satisfied by A : $\frac{1}{V_0} dA = 1$ with $V_0 = T_g^3 + 3Ah$. This leads to $A = 0.05 \text{ mm}^2 > T_g^2$. Consequently, for the periodic microstructure

considered, the volume Ah occupied by each of the three layers is greater than the one of the matrix zone strictly confined between the facets of two opposite grains. In this way, around the edges (and corners) of the grain, layers have a “common zone” that will be called “junction zone” in the following. The latter corresponds, in the general random case, to the circled zone in Fig. 1 (2D planar section).

As illustrated for the particular composite studied, the representative volume associated to the M.A. in the periodic case does not correspond to a classical unit cell (since the geometry of the whole real composite cannot be strictly reconstructed by paving the space with this cell). The periodicity is taken into account through geometrical parameters characterizing the layers and the volume V_0 may be viewed as an “equivalent” elementary “morphological pattern” proper to the Christoffersen-type approach.

3.2. Hyperelasticity of the phases

The form of the potential (i.e. the free energy per unit volume) for the matrix phase is given by the compressible Mooney–Rivlin model:

$$(3.1) \quad \omega^{\text{matrix}}(\bar{I}_1, \bar{I}_2, J) = C_{10} (\bar{I}_1 - 3) + C_{01} (\bar{I}_2 - 3) + \frac{K}{2} (J - 1)^2$$

with $\bar{I}_1 = I_1 J^{-2/3} = \text{tr}(\mathbf{C}) J^{-2/3}$, $\bar{I}_2 = I_2 J^{-4/3} = \frac{1}{2} ((\text{tr}(\mathbf{C}))^2 - \text{tr}(\mathbf{C}^2)) J^{-4/3}$, $J = (\det(\mathbf{C}))^{1/2}$. C_{10} , C_{01} and K are respectively the Mooney–Rivlin coefficients and the bulk modulus. \mathbf{C} denotes the right Cauchy–Green stretch tensor.

The grains are also supposed to display hyperelastic behavior. Their strain energy is related to the one of the matrix through a contrast coefficient as follows:

$$\omega^{\text{grain}} = \text{contrast} \times \omega^{\text{matrix}}.$$

REMARK 2. The form (3.1) of the energy is not polyconvex as shown by HARTMANN and NEFF [16]. Nevertheless, using the subroutine proposed in Abaqus[®], the stability of (3.1) in the sense of Drucker has been verified for the values of material parameters and the strain domains considered in the following.

3.3. Loading paths

The composite considered is subjected to an uniaxial compressive deformation, an incompressible tension and a simple shear, respectively defined by the

following average deformation gradients:

$$\mathbf{F}^{\text{comp}} = \begin{pmatrix} \lambda & 0 & 0 \\ 0 & 1 & 0 \\ 0 & 0 & 1 \end{pmatrix}, \quad 0.3 \leq \lambda \leq 1;$$

$$\mathbf{F}^{\text{tens}} = \begin{pmatrix} \kappa & 0 & 0 \\ 0 & 1/\kappa & 0 \\ 0 & 0 & 1 \end{pmatrix}, \quad 0 \leq \kappa \leq 2;$$

$$\mathbf{F}^{\text{shear}} = \begin{pmatrix} 1 & \beta & 0 \\ 0 & 1 & 0 \\ 0 & 0 & 1 \end{pmatrix}, \quad 0 \leq \beta \leq 0.6.$$

Practically, applying such loading paths in the morphological approach is easy: no boundary conditions have to be explicitly posed since the macroscopic deformation gradient is the only data for the corresponding localization-homogenization problem (see the end of Sec. 2.2). The periodicity of the microstructure is taken into account via the morphological parameters of the layers.

On the contrary, for the finite element modeling, defining a loading through an average deformation gradient is less evident. It cannot be used directly. In the following, it is shown that applying of such a loading can be done by imposing special conditions linking the displacements of the points located on the opposite external faces of the unit cell considered. To this end, the methodology advanced by MICHEL *et al.* [14] in the small strain framework is generalized to the finite strain one. Consider a sample constituted of multiple unit cells. Its boundary is supposed to be subjected to homogeneous deformation gradient \mathbf{F} . The resulting displacement gradient $\mathbf{h}(\mathbf{x})$ in a unit cell located far from the boundary of the sample can be decomposed as follows (\mathbf{x} denotes a point of the considered unit cell): $\mathbf{h}(\mathbf{x}) = \mathbf{H} + \mathbf{h}'(\mathbf{x})$. In the previous equation, $\mathbf{H} = \mathbf{F} - \boldsymbol{\delta}$ ($\boldsymbol{\delta}$ is the classical second-order identity tensor) is the displacement gradient that would exist in any point of any unit cell of the sample if it were homogeneous whereas \mathbf{h}' represents local fluctuations existing in the real heterogeneous material. The average of \mathbf{h}' on the unit cell vanishes so that $\langle \mathbf{h}(\mathbf{x}) \rangle_V = \mathbf{H}$ (V denotes the volume of the unit cell), and because of microstructure periodicity, \mathbf{h}' is also periodic. It can be proved that the displacement field can be split as follows:

$$(3.2) \quad \mathbf{u}(\mathbf{x}) = \mathbf{H} \cdot \mathbf{x} + \mathbf{u}'(\mathbf{x})$$

with \mathbf{u}' periodic. It is then possible to link the displacement of two opposite points P and P' (with coordinates \mathbf{x}^P and $\mathbf{x}^{P'}$) of the unit cell faces by the

following equation, resulting from (3.2) and the periodicity of \mathbf{u}' :

$$(3.3) \quad \mathbf{u}^P - \mathbf{u}^{P'} = \mathbf{H} \left(\mathbf{x}^P - \mathbf{x}^{P'} \right).$$

Thus, for each loading program defined by an average deformation gradient, Eqs. (3.3) have to be established and programmed in the F.E. modeling. The preprocessing summarized above concerning the finite element method (F.E.M.) is thus more involved than the one for the morphological approach (M.A.). Moreover, the former requires more CPU time (3400 s for the F.E.M. and 130 s for the M.A. on SG station in the case of uniaxial compressive deformation simulation).

3.4. Estimates compared to finite element results

For the comparisons presented in this section, Mooney-Rivlin coefficients and bulk modulus of the matrix are chosen as follows: $C_{10} = C_{01} = 0.5$ MPa, $K = 100$ MPa (leading to a Poisson's ratio of 0.49). The contrast between grain and matrix is 10.

For the M.A. and for each loading path previously defined, Eq. (2.5) is solved in order to find the grain deformation gradient \mathbf{f}^0 according to the methodology exposed at the end of Sec. 2.2 and using the Newton–Raphson algorithm programmed in Mathematica[®]. The knowledge of \mathbf{f}^0 allows to estimate the composite response at both scales: \mathbf{f}^α (via (2.1)) for each of the three layers defined in Sec. 3.1, the corresponding stresses in the grain and in the three layers by the local constitutive laws and finally, the homogenized nominal stress tensor \mathbf{S} via (2.4)₁.

Using F.E. modeling, local quantities (deformation gradient, first Piola–Kirchhoff stresses) are obtained at integration points. The homogenized first Piola–Kirchhoff stress tensor $\mathbf{\Pi}$ ($\mathbf{\Pi} = \mathbf{\bar{S}}^T$) is then calculated by averaging the local one over the elements constituting the unit cell.

For each of the three loading paths considered, the homogenized first Piola–Kirchhoff stress tensors will be first compared. Then, the quality of local estimates will be evaluated, notably in order to quantify –for the composite studied– the relevance of kinematical description constituting the upstream basis of the methodology. It is recalled that in the M.A., local deformation gradient is supposed to be piecewise homogeneous in the matrix (i.e. homogeneous within each of the three layers defined in Sec. 3.1), and homogeneous in the grain. Moreover, as explained in Sec. 3.1, each layer is larger than the matrix zone – designated in the following as an intergranular zone – strictly confined between the facets of the grains it separates. For more clarity, Fig. 4 provides a bi-dimensional representation of the foregoing zones in the finite element model: the black region corresponds to the intergranular zone 1 normal to \mathbf{e}^1 and the hatched one to the intergranular zone 2 normal to \mathbf{e}^2 .

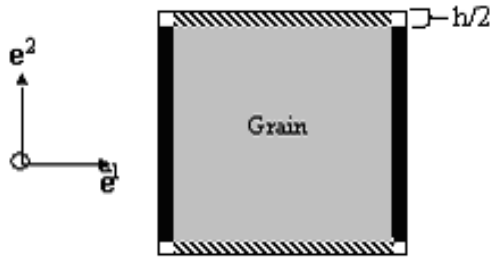


FIG. 4. Illustration of the intergranular zones in the finite element approach (2D planar section).

For quantitative evaluation of the local estimates, F.E.M “local averages” are computed in the grain and in the three intergranular zones. In this way, the homogeneous deformation gradient of layer 1 for the M.A will be compared to the average of local deformation gradients obtained at each integration point of each element of the intergranular zone 1 normal to \mathbf{e}^1 (corresponding to the black region in the bi-dimensional illustration Fig. 4). The homogeneous deformation gradient of layer 2 for the M.A will be compared to the average of local deformation gradients obtained at each integration point of each element of the intergranular zone 2 normal to \mathbf{e}^2 (hatched region in Fig. 4), the same for the intergranular zone 3 normal to \mathbf{e}^3 , not represented in Fig. 4.

3.4.1. Uniaxial compressive deformation. The composite is here subjected to uniaxial compressive strain defined by the average deformation gradient \mathbf{F}^{comp} (see Subsec. 3.3).

First, macroscopic responses are confronted. In Fig. 5, evolution of diagonal components of the homogenized first Piola–Kirchhoff stress tensor $\mathbf{\Pi}$ with loading factor λ is given. Considering the geometry of the periodic microstructure and the loading symmetry, there is $\Pi_{22} = \Pi_{33}$. Compared with homogenized responses obtained by F.E. modeling, macroscopic estimates given by M.A. are highly relevant (greatest relative error $= 100 \times \frac{|\Pi_{11}^{M.A.} - \Pi_{11}^{F.E.M.}|}{|\Pi_{11}^{F.E.M.}|}$ is inferior to 3%).

In order to discuss the pertinence of the hypothesis of piecewise homogeneity of local deformation gradient \mathbf{f} , the diagonal components of \mathbf{f} for the unit cell, obtained by the F.E. calculations have been examined. All along the loading concerned, it appears that local heterogeneity is located near the edges of the unit cell, namely near the edges of the grain (in the intergranular zones coming close to the “junction zones” and in the “junction zones” themselves). This feature is illustrated in Fig. 6 for a load factor λ equal to 0.72.

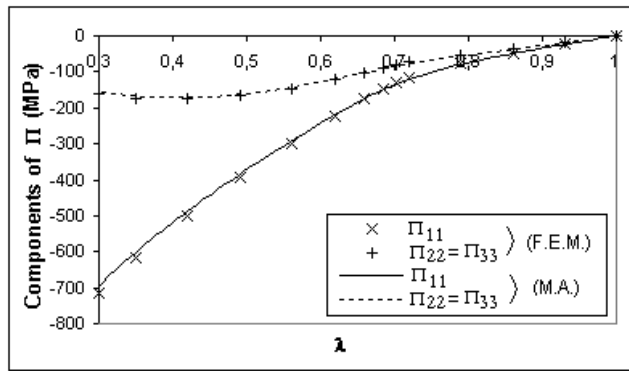


FIG. 5. Comparison of homogenized stresses Π_{11} and $\Pi_{22} = \Pi_{33}$ obtained by both methods (F.E.M. and M.A.) for simulated uniaxial compressive deformation.

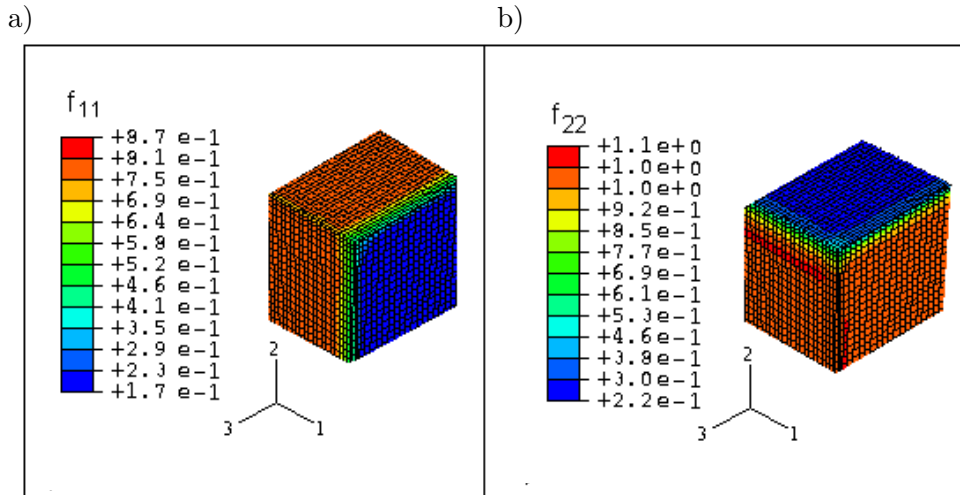


FIG. 6. F.E.M.: diagonal components of local deformation gradient \mathbf{f} for the eighth of the unit cell (3D view) during simulated uniaxial compressive deformation ($\lambda = 0.72$): a) f_{11} ; b) f_{22} .

Looking also *into* the unit cell one can conclude that in the grain, and in each intergranular zone, the deformation gradient can be considered to be homogeneous and this, all along the loading. Indeed, no significant heterogeneity is noticed in the grain and the extent of heterogeneity that may be observed in each of the three intergranular zones in the very close neighborhood of the grain edges, namely when coming close to the “junction zones”, remains limited. Fig. 7a and b, showing respectively the 11 and 22 components of deformation gradient in the middle plane of the unit cell orthogonal to \mathbf{e}^3 for $\lambda = 0.86$ provides an illustration of this feature.

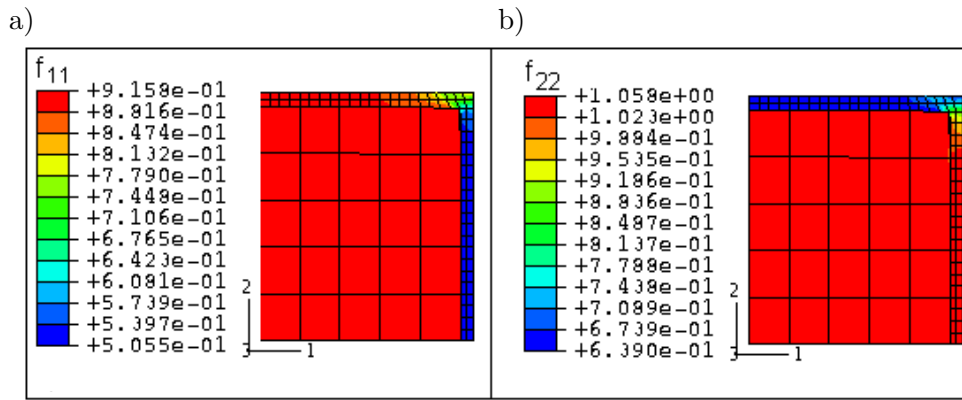


FIG. 7. F.E.M.: diagonal components of local deformation gradient \mathbf{f} in a quarter of the unit cell (2D planar section) during simulated uniaxial compressive deformation ($\lambda = 0.86$): a) f_{11} ; b) f_{22} .

Figure 8 compares the average principal stretches, in directions 1 and 2, in the intergranular zones and in the grain obtained by both methods (see explanations in Sec. 3.4). The results of the F.E.M. are represented by crosses and the ones of the M.A. by solid lines.

One may observe a good agreement all along the loading. Indeed, except for intergranular zone 1 in the direction 1, respectively 2 in the direction 2, for which a maximum relative error of 14% is selectively reached (for $0.65 < \lambda < 0.7$), the error is less than 3%. This shows a small effect of strain heterogeneity observed in the three intergranular zones on their average strain states and furthermore, the quantitative accuracy of local stretches estimated by the M.A. in these regions and in the grain.

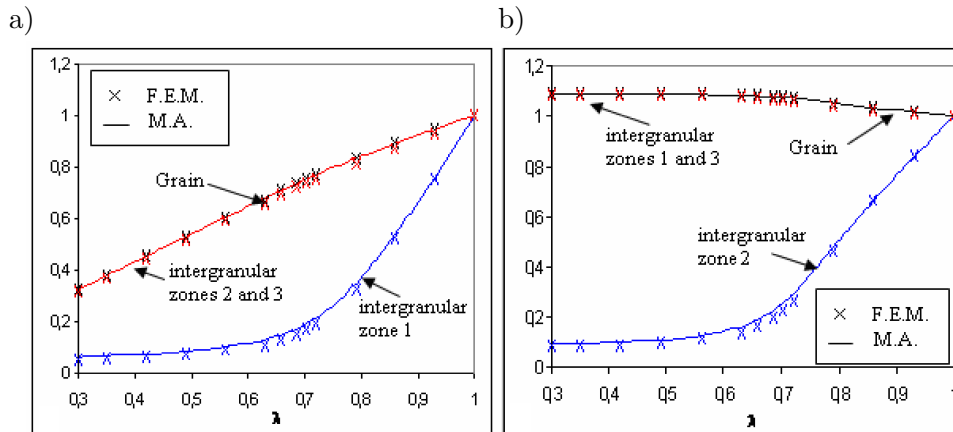


FIG. 8. Local average principal stretches for simulated uniaxial compressive deformation: a) in direction 1; b) in direction 2.

In direction 1, all constituents (grain and intergranular zones) are compressed. As expected, the intergranular zone 1 normal to the direction of compression is the most compressed. Moreover, the stretches of intergranular zones 2 and 3 are identical due to the geometry-and-loading symmetry (see also Fig. 6a). For the M.A. these stretches are exactly equal to the stretch of the grain. Indeed, using Eq. (2.1) with the morphological parameters defined at the end of Sec. 3.1, one obtains: $f_{11}^{\text{layer-}i} = f_{11}^0$ for $i = 2, 3$. Regarding the F.E. modeling, it is also the case in the parts where the stretches are homogeneous, namely everywhere except very close to the “junction zones”. This is illustrated by the cartography of Fig. 7a where most of the elements of the intergranular zone 2 are shown to have the same contraction as the grain in the direction 1. Contrary to what was expected by the authors of [5] before confrontation, this feature is in fact fully relevant. The very slight difference in Fig. 8a between red crosses (for intergranular zones 2 and 3) and black crosses (for the grain) in the direction 1 shows the very small influence of strain heterogeneity in intergranular zones induced by the effects in the “junction zones”.

In direction 2 (see Fig. 8b), the intergranular zone 2 is compressed whereas the grain and the other intergranular zones are stretched. Due to the geometry-and-loading symmetry, the intergranular zones 1 and 3 have the same stretches in this direction (see also Fig. 6b for F.E.M). Moreover, according to the M.A. the following equality is given by Eq. (2.1): $f_{22}^{\text{layer-}i} = f_{22}^0$ for $i = 1, 3$ since $\mathbf{d}^1 = d \mathbf{e}^1$ and $\mathbf{d}^3 = d \mathbf{e}^3$. It is also the case in the F.E.M. as illustrated by Fig. 7b where the intergranular zone 1 is seen to have almost everywhere the same stretch in direction 2 as the grain.

Local stretches in direction 3 are not given since they do not provide additional information. Actually, in direction 3 the conclusions are analogous to those for direction 2, except that the roles of intergranular zones 2 and 3 are inverted.

Figure 9 representing evolution of the local average first Piola-Kirchhoff stresses (components 11 and 22) with macroscopic loading factor λ , shows the relative pertinence of the M.A. compared with the F.E.M. regarding the local response estimates. As for the stretches, the greatest relative error in the direction 1, respectively 2, is obtained for the intergranular zone 1, respectively 2. It increases progressively to attain a maximum of 18%.

As a conclusion, except for the matrix zones not comprised between the grain facets (“junction zones”) and in a very close neighborhood of these zones, local stretches estimated by the M.A. are satisfactory when compared to the “exact” F.E. solution. Moreover, the local average stresses are correctly estimated. One may emphasize that the absence of a correct description of the local effects in the “junction zones” does not affect (for the loading and microstructure considered) the quality of the estimates obtained at both scales.

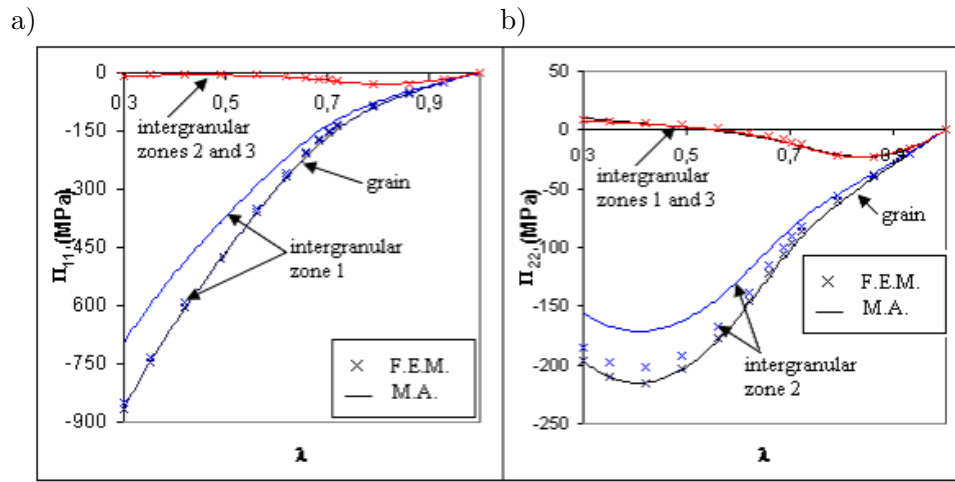


FIG. 9. Local average first Piola-Kirchhoff stresses for simulated uniaxial compressive deformation: a) in direction 1; b) in direction 2.

3.4.2. Incompressible tension. As a first illustration of the M.A to deal with incompressible loading paths, the composite is subjected here to an incompressible tension defined by the average deformation gradient \mathbf{F}^{tens} (see Sec. 3.3). The macroscopic responses obtained by both methods are compared (see Fig. 10 representing the homogenized first Piola–Kirchhoff stresses as a function of loading factor κ). From a macroscopic viewpoint, the estimates obtained via M.A. are satisfactory approximations of the numerical solution given by the F.E.M. (maximum relative error = $100 \times \frac{|\Pi_{22}^{M.A.} - \Pi_{22}^{F.E.M.}|}{\Pi_{22}^{F.E.M.}} = 5.9\%$).

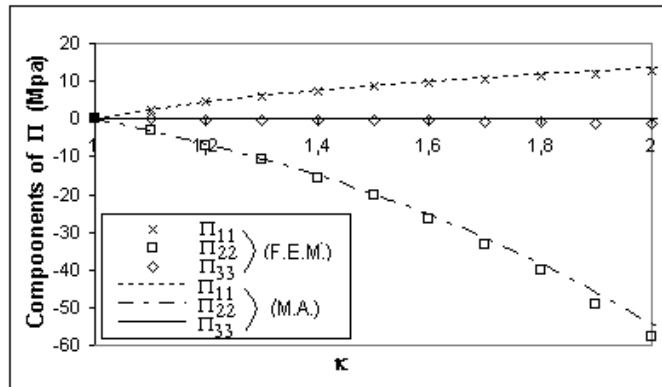


FIG. 10. Comparison of homogenized stresses Π_{11} , Π_{22} , and Π_{33} obtained by both methods (F.E.M. and M.A.) during simulated incompressible tension.

When examining the local strain heterogeneity within the grain and each of the three intergranular zones, it appears more pronounced – in terms of extent – than for a uniaxial compressive loading path (Subsec. 3.4.1). In particular, strain heterogeneity observed in each of the three intergranular zones may not be located in the very close neighborhood of the “junction zones”, as illustrated in Fig. 11 showing the distribution of f_{11} through the unit cell for $\kappa = 1.5$.

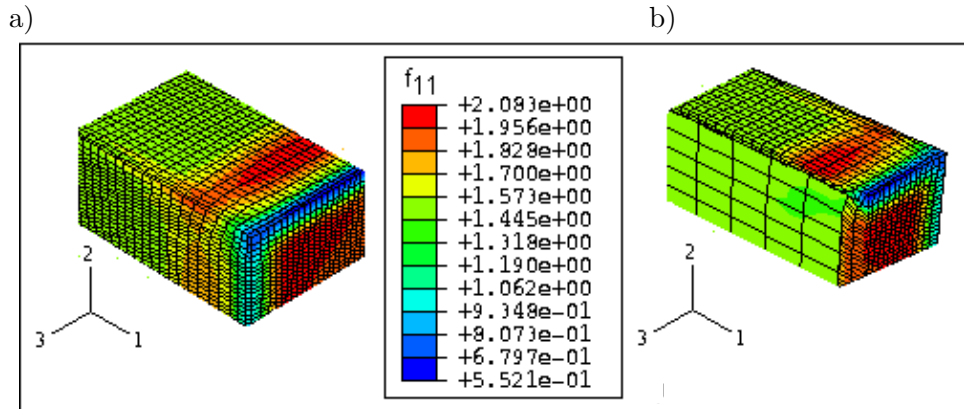


FIG. 11. F.E.M.: component 11 of local deformation gradient for simulated incompressible tension ($\kappa = 1.5$) a) eighth of the unit cell (view on the matrix); b) in the unit cell (planar section normal to \mathbf{e}^3).

In order to exemplify the relevance of local estimates, Fig. 12 presents the average principal stretches in intergranular zone 1 where the correlation between M.A. and F.E. results is less significant (compared with that obtained for grain and intergranular zones 2 and 3). As it can be seen, a good quantitative agreement is nevertheless obtained in the directions 2 and 3. The greatest relative error is obtained in the direction 1: it increases to attain 10% for $\kappa = 1.5$ and 15% at the end of the loading. The deformed shapes of the structure for two different loading factors during the simulation are also given in Fig. 12. It is shown that the elements in intergranular zone 1 are considerably deformed.

So, even if the hypothesis of piecewise homogeneity of the local deformation gradient in the matrix phase is here less evident than for the uniaxial compressible loading path previously studied, the M.A. provides nevertheless an acceptable approximation of the average strain state in the grain and in each intergranular zone. Moreover, one may note once again, that the absence of a correct description of the junction zones does not affect the quality of the estimates at the macroscopic level (see Fig. 10).

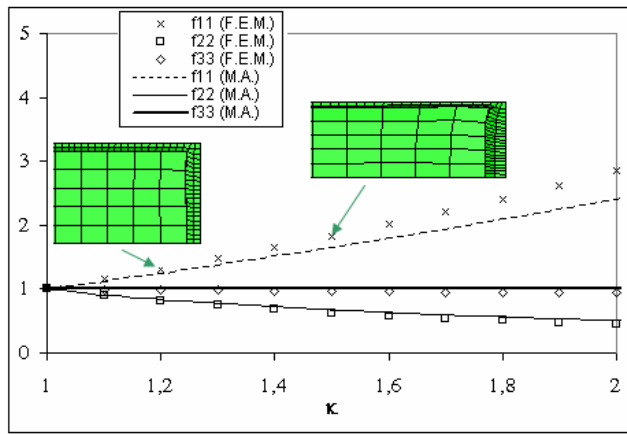


FIG. 12. Average principal stretches in intergranular zone 1 (M.A. and F.E.M.) as functions of κ and associated deformed shape (F.E.M.) of a quarter of the unit cell (2D planar section), for simulated incompressible tension.

3.4.3. Simple shear loading. A simple shear loading defined by $\mathbf{F}^{\text{shear}}$ (see Subsec. 3.3), is now considered. The maximum macroscopic loading level is $\beta = 0.6$. The strong distortion of zones A and B illustrated in Fig. 13 shows how such a loading path is severe for the microstructure considered.

Components 12 and 21 of the homogenized first Piola–Kirchhoff stress tensor $\mathbf{\Pi}$ as functions of β are given in Fig. 13. As it can be seen, M.A. results concerning Π_{12} are satisfactory (relative error is selectively equal to 7.7% for $\beta = 0.3$ smaller than 6% otherwise), whereas Π_{21} is poorly approximated for $\beta > 0.3$.

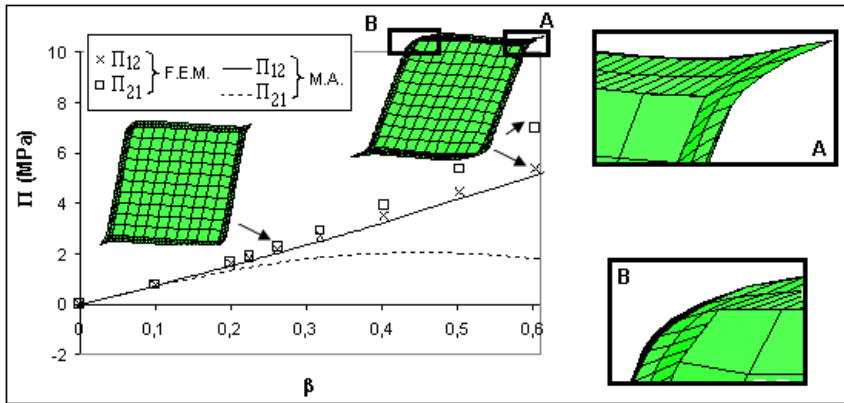


FIG. 13. Comparison of homogenized stresses Π_{12} and Π_{21} obtained by both methods (F.E.M. and M.A.) and associated deformed shape (F.E.M.) of the unit cell (2D planar section), during simulated simple shear.

Local deformation gradients have been examined in all the regions of the unit cell (grain, each of the three intergranular zones, “junction zones”) all along the loading. First, the hypothesis of homogeneous deformation gradient for the grain is debatable especially for component 21. The agreement between the F.E.M. and M.A. results is nevertheless good for all the components (relative error less than 2 %) except for the 21 component for which the error increases progressively to attain 20% at the end of the loading.

As for the uniaxial compressive loading path, the heterogeneity in each of the three intergranular zones – due to effects in the junction zones – remains located in a very close neighborhood of the grain edges (low extent). On the contrary, the effect of this heterogeneity is not always negligible. Such a situation is particularly pronounced for f_{21} in the intergranular zones 2 and 3. As illustrated by the cartography 3D in Fig. 14 for $\beta = 0.3$, the value of f_{21} in the homogeneous regions (blue in Fig. 14) is much lower than the corresponding values near

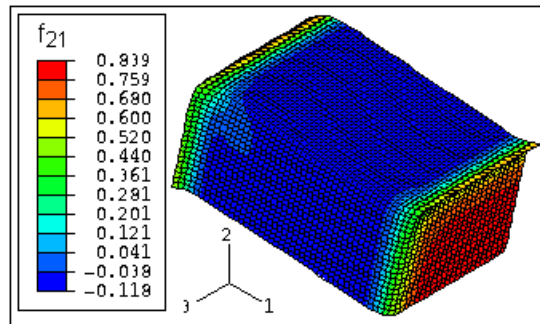


FIG. 14. F.E.M.: component 21 of local deformation gradient for simulated simple shear ($\beta = 0.3$) in a quarter of the unit cell (view on the matrix).

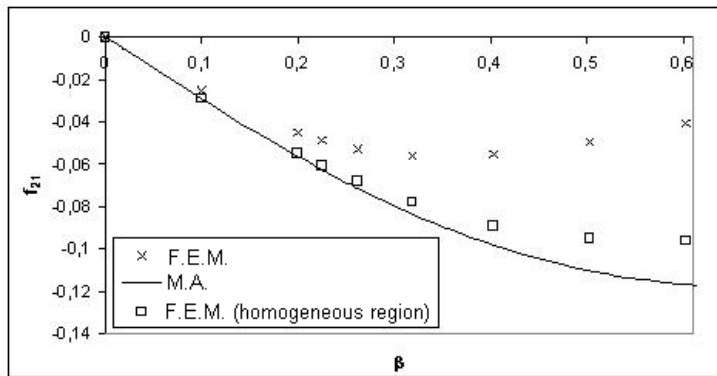


FIG. 15. Component 21 of local deformation gradient in intergranular zone 2 for simulated simple shear: average and point-wise value in the homogeneous region (F.E.M.), estimated value (M.A.).

the “junction zones” with the intergranular zone 1. The average values of f_{21} in intergranular zones 2 and 3 are highly influenced by this heterogeneity (despite its low extent) and are poorly approximated by M.A. (error greater than 50 %). It is to be noted that M.A. approximation is in better agreement with point-wise F.E. estimation in the homogeneous blue region in Fig. 14. The foregoing features are illustrated for the intergranular zone 2 by the curves presented in Fig. 15. The relative error between the estimate and the local (point-wise) value in the homogeneous region is here around 10%.

For the other components of the deformation gradient, the agreement is better. When the heterogeneity, slightly extended in the intergranular zones, has no significant influence on the average values (which therefore are close to the values in the homogeneous parts), there is a good convergence between the F.E.M. and M.A. results (relative error lower than 6 %). Such a situation concerns all the components, except f_{22} in intergranular zone 2 and f_{12} in intergranular zone 3, for which the errors remain nevertheless acceptable (around 15% at the end of the loading). For illustration, Fig. 16 presents the confrontation results for f_{12} .

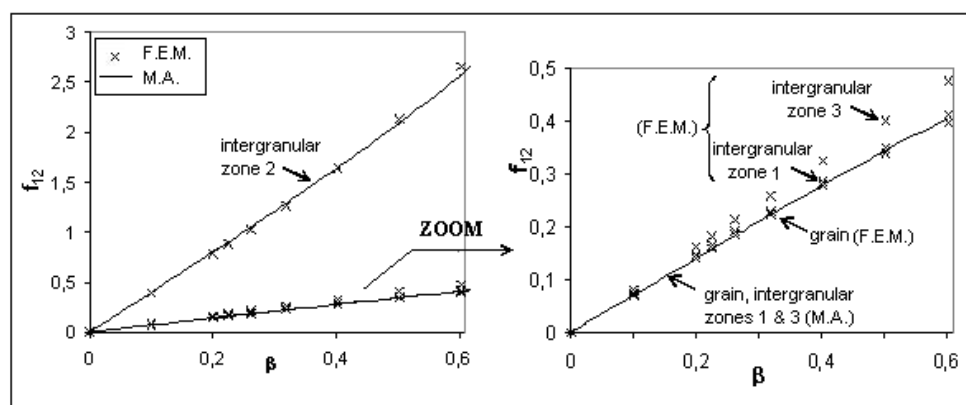


FIG. 16. Average local deformation gradient (component 12) for simulated simple shear.

The scope of the present paper (triple loading path, three-dimensional, local/global M.A./F.E. comparison and evaluation in finite elasticity plus, in Sec. 4 further, viscohyperelastic direct treatment, algorithm and application) did not reasonably allow us to open in this text another issue, namely the problem of incompressibility. This issue, i.e. the eventual incompressibility constraint for respective phases and/or for the global response, may be considered as one of the probing criteria for scale transition modelling in the context of (visco)-hyperelasticity (see for example [25]). We let the Reader with the preliminary analysis regarding effect of the Poisson ratio for the matrix material on the 21 component of \mathbf{f}^0 under simple shear (see Fig. 17). The Poisson ratio effect is

studied within the interval $[0.41, 0.4995]$. The 21 component values of \mathbf{f}^0 vs the loading parameter β illustrate here the fact that the M.A. response appears more sensitive to Poisson's ratio close to the incompressibility limit than the F.E. solution. To explain this effect further simulations are necessary, possibly involving varying contrast and more complex microstructures. This is the subject of prospective works.

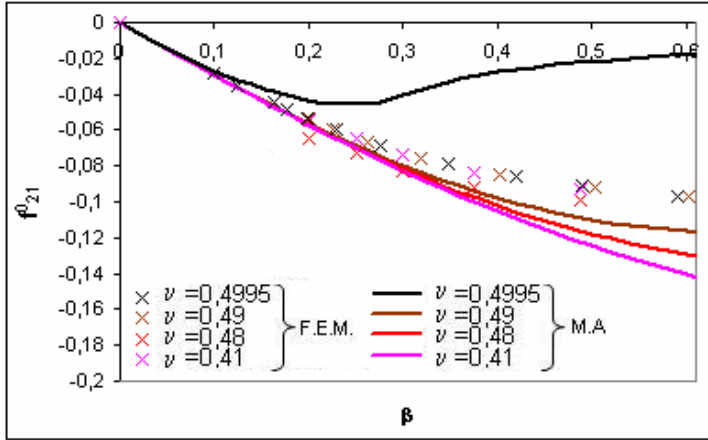


FIG. 17. Average local deformation gradient in the grain (component 21) for simple shear simulations (F.E.M. and M.A.) with different Poisson ratio ν .

3.4.4. Discussion. Parallel setting of uniaxial compressive deformation and simple shear for the three-dimensional albeit regular microstructure under consideration, allows for the first quantitative evaluation of the potentialities and limits of the kinematic prerequisite of the M.A.. In particular, some remarks can be made about the role of the junction zones. In a way, for both loading paths, the heterogeneity of deformation in the intergranular zones is preponderantly due to what happens in the junction zones. For the uniaxial compressive deformation, the junction zones are involved to a lesser degree in aggregate deformation features, and the M.A. provides good estimation of local fields. The situation is more contrasted for the simple shear where junction zones take a major part of deformation (see Figs. 13, 14 for this effect in “horizontal” junction zones). This event and the corresponding influence on the distribution of heterogeneities in the intergranular zones cannot be neglected notably for the 21 component of the deformation gradient. Consequently, the corresponding local average values are poorly estimated.

Moreover, the hypothesis of homogeneity in the grain is questionable for this second loading path. Despite it, it can be conjectured that the results obtained

allow to qualify globally the method as a promising one. More general situations including random microstructures should be considered to clarify the statement. It is expected that for random configurations of intergranular zones, the role of the junction zones will be less pronounced than for the periodic microstructure under simple shear. It is to be reminded that the method is destined primarily to treat random microstructures. Finally, when comparing the grain morphology assumed within the M.A. framework with the class of engineering composites at stake (smoother grains), it is evident that the effect of sharp edges of polyhedral grains inherent to M.A. tends to accentuate the concentration in the junction zones in F.E. calculations. Paradoxically, the material response given via M.A. (which introduces the sharp edges of grains while considering the deformation homogeneous in the layers) may be closer to the F.E. solution for the composite with blunt grains than to the F.E. evaluation with polyhedral grains. This conjecture is to be confirmed in forthcoming studies focusing specifically on geometrical features.

4. Application to visco-hyperelasticity

In the nonlinear homogenization framework, the treatment of time-dependent behavior where both elastic and viscous effects coexist (viscoelasticity, elastoviscoplasticity) still constitutes a challenge (see BORNERT *et al.* [17] for example). First of all, the difficulty linked to the description of space-time couplings between the constituents and their macroscopic consequence – the so-called “long-range memory effect” (see SUQUET [4]) – has been shown in some works. Second, the strong influence of the microstructure (finely linked to local heterogeneity) on the macroscopic response for heterogeneous viscoelastic composites has been highlighted (see for example BEURTHEY and ZAOUI [3]). Finally, most of the current classical approaches make use of the correspondence principle and the Laplace-Carson transform to deal with viscoelastic composites. Except for very particular microstructures, it results in highly involved calculations, notably when proceeding with the inversion of the Laplace-Carson transforms. New methods have been recently proposed to simplify the numerical treatment of viscoelastic composites (see the “time integration approach” proposed by LAHELLEC and SUQUET [18] and the “direct inversion method” advanced by BRENNER and MASSON in [19]).

In this context, Christoffersen’s original approach has been extended to small strain viscoelasticity by NADOT *et al.* [2]. In a direct manner –namely without using the Laplace-Carson transforms– qualitatively satisfactory results were obtained in terms of local viscoelastic interactions and consequent long-range memory effect. Considering also the encouraging relevance of the first results obtained in the finite strain framework (see Sec. 3.4), the objective is here to

apply the M.A. (Sec. 2) to viscohyperelasticity. Such a behavior is indeed far more representative of the mechanical response displayed by the materials (energetic composites) to which the M.A. is devoted.

After a brief presentation of the thermodynamic viscohyperelastic law of the matrix phase (Sec. 4.1), the direct numerical local problem solving procedure, complying with the methodology presented in Sec. 2.2, is detailed. Finally, the first results obtained for the particular periodic microstructure presented in Sec. 3.1 are presented.

4.1. Viscohyperelastic model

In order to describe the viscoelasticity of the matrix, a thermodynamic approach with internal variable, based on the previous works of TRUMEL *et al.* [20, 21], is used. The additive decomposition of both thermodynamic potential w and the second Piola–Kirchhoff stress tensor \mathbf{S} into an elastic part (superscript (r)) and a viscous part (superscript (v)) is assumed, as proposed for example by REESE and GOVINDJEE [22]:

$$w = w^{(r)} + w^{(v)}; \quad \mathbf{S} = \mathbf{S}^{(r)} + \mathbf{S}^{(v)}.$$

The reversible (equilibrium) and viscous (non-equilibrium) parts of \mathbf{S} are obtained by partial differentiation of the free energy w with respect to the state variables \mathbf{E} (Green–Lagrange strain tensor) and $\boldsymbol{\gamma}$ (symmetric strain-like internal variable describing the dissipative viscoelastic relaxation process) respectively:

$$\mathbf{S}^{(r)} = \frac{\partial w}{\partial \mathbf{E}}, \quad \mathbf{S}^{(v)} = \frac{\partial w}{\partial \boldsymbol{\gamma}}.$$

The hyperelastic part $\mathbf{S}^{(r)}$ is described by the constitutive law presented in Sec. 3.2 (Eq. (3.1)) while the viscous part $\mathbf{S}^{(v)}$ is assumed to be linear in $\boldsymbol{\gamma}$ as follows: $\mathbf{S}^{(v)} = \mathbf{L}^{(v)} : \boldsymbol{\gamma}$, where $\mathbf{L}^{(v)}$ is a fourth-order tensor of viscous moduli. The evolution of the internal variable $\boldsymbol{\gamma}$ is assumed to be given by the following Eq. (4.1), where τ denotes a unique relaxation time and $\overline{\mathbf{E}}$ the time-derivative of the deviatoric part of \mathbf{E} :

$$(4.1) \quad \dot{\boldsymbol{\gamma}} + \frac{1}{\tau} \boldsymbol{\gamma} = \overline{\mathbf{E}}; \quad \boldsymbol{\gamma}(t=0) = \mathbf{0}.$$

The form of (4.1) ensures the thermodynamic admissibility for the model (positive viscoelastic dissipation). More comments concerning this viscoelastic model can be found in [2, 20, 21].

4.2. Numerical solution

In accordance with the methodology exposed at the end of Sec. 2.2, the local constitutive relations for the matrix and the grains are included in Eq. (2.5). The grains are here considered hyperelastic, using the compressible Mooney–Rivlin model described in Sec. 3.2 and the matrix viscohyperelastic, following the constitutive relationships defined in the above section. It is reminded that in the approach considered (i.e. the M.A.), the matrix is generally schematized by an assembly of layers with different thicknesses and orientations. As stressed in Sec. 2.2, the deformation gradient in layer α , depending explicitly on the morphological parameters proper to layer α (see Eq. (2.1)), is different from the deformation gradient in another layer. Thus, a different Green-Lagrange strain tensor is associated with each layer; it is denoted by \mathbf{E}^α for layer α ($\mathbf{E}^\alpha = 1/2 (\mathbf{f}^{\alpha T} \mathbf{f}^\alpha - \boldsymbol{\delta})$).

Consequently $\dot{\bar{\mathbf{E}}}$ also varies from one layer to another, which means (via (4.1)) that each layer has its proper current relaxation state, denoted $\boldsymbol{\gamma}^\alpha$ for the layer α . Furthermore, as many internal variables as the number of layers are required to deal with the whole relaxation state of the matrix phase. In this way, when introducing local constitutive laws, Eq. (2.5) – used to determine the unknown \mathbf{f}^0 – is to be completed by a time-differential system relative to the evolution of all the internal variables. More precisely, the following equations must be solved simultaneously:

$$(4.2) \quad \begin{aligned} (1-c) \bar{s}_{Ji}^0 + \frac{1}{V_0} \sum_{\alpha} \bar{s}_{Ji}^{\alpha} A^{\alpha} h^{\alpha} - \frac{1}{V_0} \sum_{\alpha} \bar{s}_{Ki}^{\alpha} n_K^{\alpha} A^{\alpha} d_J^{\alpha} &= 0, \\ \dot{\gamma}_{KL}^{\alpha} + \frac{1}{\tau} \gamma_{KL}^{\alpha} &= \dot{\bar{E}}_{KL}^{\alpha}; \quad \gamma_{KL}^{\alpha}(t=0) = 0 \quad \forall \alpha, \end{aligned}$$

where

- (i) \bar{s}^0 is a function of \mathbf{f}^0 ;
- (ii) \bar{s}^{α} for each layer α is a function of \mathbf{f}^0 , \mathbf{F} , the given macroscopic deformation gradient and the internal variable $\boldsymbol{\gamma}^{\alpha}$ (via (2.1) in addition to the matrix law);
- (iii) $\bar{\mathbf{E}}^{\alpha}$ for each layer α is a function of \mathbf{f}^0 and \mathbf{F} (via (2.1)).

All the equations constituting System (4.2) are thus strongly coupled. In order to solve (4.2), the following particular algorithm has been developed.

The starting point consists in considering that the unknown grain deformation gradient \mathbf{f}^0 varies linearly with time for each time step considered (which is an acceptable strategy if the chosen time step is sufficiently small). Consider the time step n . The initial values \mathbf{f}_{n-1}^0 and $\boldsymbol{\gamma}_{n-1}^{\alpha}$ for each layer α are known (for the first time step i.e. for the non deformed and perfectly relaxed material,

$\mathbf{f}_0^0 = \boldsymbol{\delta}$, $\boldsymbol{\gamma}_0^\alpha = \mathbf{0} \forall \alpha$, and for the following steps, these values have been calculated at the previous time step). With the foregoing assumption, $\dot{\bar{\mathbf{E}}}_n^\alpha$ for each layer α is expressed in function of unknown final value \mathbf{f}_n^0 of \mathbf{f}^0 . Each internal variable $\boldsymbol{\gamma}_n^\alpha$ is then expressed as a function of unknown \mathbf{f}_n^0 through Eqs. (4.2)₂. Reporting all these expressions in (4.2)₁, \mathbf{f}_n^0 is numerically calculated using the Newton–Raphson subroutine proposed in Mathematica[®]. Once \mathbf{f}_n^0 is determined, numerical values of internal variables at time $t_n - \boldsymbol{\gamma}_n^\alpha \forall \alpha$ – are computed; they are used together with \mathbf{f}_n^0 as initial conditions for the next time step. By doing so, numerical values for deformation gradient \mathbf{f}^0 and viscoelastic variables $\boldsymbol{\gamma}^\alpha$ are known at each time t_n and, consequently, every local or global quantity can be computed following the methodology exposed at the end of Sec. 2.2.

4.3. First estimates

In order to illustrate the ability of the morphological approach (M.A.) to deal with viscohyperelasticity, the previous general algorithm is processed for the microstructure proposed in Sec. 3.1. The coefficients used to describe the reversible part of matrix behavior (hyperelasticity) are taken from the literature (HEUILLET and DUGAUTIER [23]) as follows: $C_{10} = 0.21$ MPa, $C_{01} = 0.02$ MPa, and $K = 100$ MPa, and for the grain: $C_{10}^0 = 2.1$ MPa, $C_{01}^0 = 2.1$ MPa and $K^0 = 1000$ MPa (contrast of 10). Concerning the viscous part of the matrix behavior, $\mathbf{L}^{(v)}$ is supposed to be isotropic and defined by $E^{(v)} = 50$ MPa and $\nu^{(v)} = 0.49$; at last, $\tau = 15$ s.

According to the model at stake, the truly viscoelastic effects affect the deviatoric part of the strain tensor \mathbf{E}^α . That is why the application presented in the following involves the simple shearing loading/unloading path, despite the fact that the corresponding hyperelastic confrontation M.A./F.E. presented in Sec. 3 is less satisfactory than the one for uniaxial compressive deformation. The

deformation gradient is then $\mathbf{F}^{\text{shear}} = \begin{pmatrix} 1 & \beta & 0 \\ 0 & 1 & 0 \\ 0 & 0 & 1 \end{pmatrix}$ with $0 \leq \beta \leq 2, \beta = v.t$; v

denotes shearing velocity.

In Fig. 18, evolution of homogenized first Piola–Kirchhoff shear stresses Π_{12} with loading factor β is given for two loading velocities: the bold line corresponds to $v = 5.10^{-3}\text{s}^{-1}$ and the thin one to the lowest velocity $v = 2.10^{-3}\text{s}^{-1}$. Experimentally observed phenomena, such as increase of stiffness and hysteresis dependent on the loading velocity, are qualitatively well predicted by the M.A..

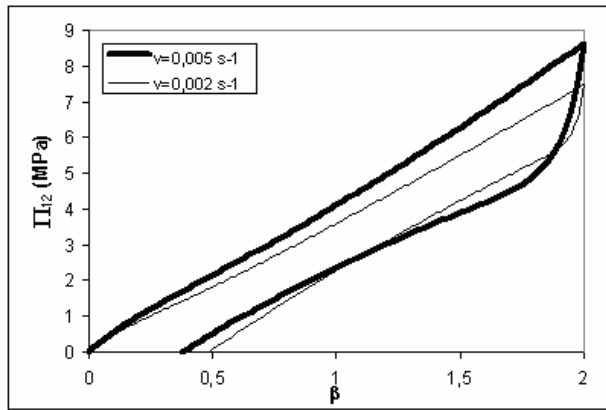


FIG. 18. M.A. simulations for two shear rates ν : homogenized stresses Π_{12} for simple shear loading.

5. Conclusion

The purpose of this paper was to provide the first quantitative evaluation in the finite strain framework of a non-classical scale transition methodology for highly-filled particulate composites – the so-called “morphological approach” (M.A.), and to show its possible applicability in the context of time-dependent behavior such as viscohyperelasticity. This approach, consisting in the generalization to finite strain performed by GUIOT *et al.* [5] of the earlier linear framework by CHRISTOFFERSEN [1], makes use of two essential incipient stages for the further localization-homogenization process. The first stage, consisting in “geometrical schematization”, represents the real composite microstructure by an aggregate of polyhedral grains separated by thin layers of matrix. Salient information on the morphology of the real material – regarding spatial arrangement and shape of the grains, preferential orientations of the interfaces – is conserved through the definition of “morphological parameters”. The second stage, called “kinematical schematization”, consists in simplifying assumptions concerning the local motion within the foregoing grain/layers aggregate. As a result of this starting procedure, the deformation gradient in a layer of matrix is explicitly related to the morphological parameters of the considered layer; some strain heterogeneity is then described in the matrix phase viewed as an assembly of layers with different morphological parameters. Another advantage lies in the simple accessibility to an estimate of local fields (everywhere except around grain edges) in a nonlinear context (regarding kinematics and constitutive laws).

Moreover, most of existing nonlinear homogenization schemes are referred to the notion of equivalent linear composite and need prior linearization of the constitutive behavior. This linearization procedure and the choice of the definition of the linearized moduli are two sources of approximation, which have a strong influence on the global estimates (see e.g. REKIK *et al.* [24], MOULINEC and SUQUET [8]). Is it noticeable that for the M.A. the nonlinear constitutive laws do not need any prior modification.

In order to evaluate the relevance of the kinematical description in a geometrically nonlinear context (finite deformation), M.A. global and local estimates have been compared to the finite element results for a three-dimensional composite with periodic microstructure and hyperelastic constituents described by compressible Mooney–Rivlin laws. Very good results at both scales are obtained for uniaxial compressive deformation whereas they are less satisfactory under a simple shear. For the latter loading path, the hypothesis of homogeneity of deformation gradient in the grain and the absence of a correct description of effects in the junction zones appear as limits.

An important technical advantage of the M.A. is that periodicity conditions relative to the geometry of the microstructure are “naturally” taken into account and that the loading is applied by imposing simply the macroscopic deformation gradient. On the contrary, in the finite element method, the periodicity and the “average loading” require a specific preprocessing procedure regarding the degrees of freedom of the external nodes of the unit cell, that must be re-established for every new loading case. Moreover, the CPU time required by the M.A. is much smaller than for the F.E. analysis.

As the M.A. is addressed in the long-run to deal with energetic composites, its ability to treat viscohyperelasticity (which characterizes the behavior displayed notably by the matrix phase in these materials) has been shown. The numerical solving procedure relative to the corresponding localization-homogenization problem, in the general case of a random microstructure, is put forward by means of a specific algorithm able to treat the coupling induced by the relaxation internal variables. As for the recent method proposed by LAHELLEC and SUQUET [18], the solving procedure at stake regards directly the time-domain. It is a step-by-step procedure where all the quantities at the end of the time step are deduced only from those at the beginning of the step.

If qualitatively satisfactory results have been obtained at a macroscopic scale in viscohyperelasticity for the three-dimensional periodic microstructure previously considered, the quantitative relevance has to be evaluated further. This will be done once again by confronting both the global and local estimates, with the finite element results for loading paths for which the M.A. estimates are good in hyperelasticity.

As a future work, more complex (random) microstructures will be considered in order to come closer to the engineering composites. These microstructures will be numerically generated in order to respect the requirements of the geometrical schematization (polyhedral grains, parallelism of opposite interfaces). According to the application context, some predominance will be given to highly compressive loading paths. So, even if some matrix intergranular zones are subjected to sliding, one may hope that the contribution of the “junction zones” to the strain state of the random aggregate will be weaker than for the periodic microstructure under simple shear. Moreover, it will be interesting to quantify the influence of the hypothesis of identical deformation gradient for all grains whose eventual limits could not be evaluated in the periodic case studied before. Such prospective studies, for random microstructures and also different contrasts, involving further parallel M.A./F.E.M. computations, should definitely quantify the validity domain of the kinematical description constituting the very basis of the scale transition at stake and the origin of its specificity and main advantages.

In parallel, some investigations are under way regarding the crucial geometrical schematization step for a real propellant-like composite material. X-ray tomography together with available tools of morphological analysis of 3D images, are being used to optimize the correspondence of ‘true’ microstructure with the Christoffersen-like one, from which the morphological parameters required by the M.A. have to be identified. Afterwards, comparisons with experimental results will be searched for a real propellant.

Acknowledgments

Fruitful discussions with J.C. Michel (Laboratoire de Mécanique et d’Acoustique/CNRS, Marseilles, France) regarding F.E. calculations are gratefully acknowledged as well as the financial support from the French Ministry of Defence.

References

1. J. CHRISTOFFERSEN, *Bonded granulates*, J. Mech. Phys. Solids, **31**, 55–83, 1983.
2. C. NADOT-MARTIN, H. TRUMEL, A. DRAGON, *Morphology-based homogenization for viscoelastic particulate composites: Part I: Viscoelasticity sole*, Eur. J. Mech. A/Solids, **22**, 89–106, 2003.
3. S. BEURTHEY, A. ZAOUI, *Structural morphology and relaxation spectra of viscoelastic heterogeneous materials*, Eur. J. Mech. A/Solids, **19**, 1–16, 2000.
4. P. SUQUET [in:], *Homogenization techniques for composite media*, E. Sanchez-Palencia, A. Zaoui [Eds.], Springer, Berlin 1987.

5. B. GUIOT, C. NADOT–MARTIN, A. DRAGON, *Towards a nonlinear micromechanics-based analysis for particulate composites*, Composites Science and Technology, **66**, 2726–2735, 2006.
6. S. NEMAT-NASSER, M. HORI, *Micromechanics: overall properties of heterogeneous materials*, Elsevier Science Publishers B.V., The Netherlands 1993.
7. M. BORNERT, *A generalized pattern-based self-consistent scheme*, Computational Materials Science, **5**, 17–31, 1996.
8. H. MOULINEC, P. SUQUET, *Intraphase strain heterogeneity in non linear composites: a computational approach*, Eur. J. Mech. A/Solids, **22**, 751–770, 2003.
9. P. PONTE–CASTAÑEDA, *Second-order homogenization estimates for nonlinear composites incorporating field fluctuations: I–theory*, J. Mech. Phys. Solids, **50**, 737–757, 2002.
10. P. PONTE–CASTAÑEDA, *Second-order homogenization estimates for nonlinear composites incorporating field fluctuations: II–applications*, J. Mech. Phys. Solids, **50**, 759–782, 2002.
11. M.I. IDIART, P. PONTE–CASTAÑEDA, *Field fluctuations and macroscopic properties for nonlinear composites*, Int. J. Solids Structures, **40**, 7015–7033, 2003.
12. M.I. IDIART, H. MOULINEC, P. PONTE–CASTAÑEDA, P. SUQUET, *Macroscopic behavior and field fluctuations in viscoplastic composites: Second-order estimates versus full-field simulations*, J. Mech. Phys. Solids, **54**, 1029–1063, 2006.
13. H. MOULINEC, P. SUQUET, *A numerical method for computing the overall response of non linear composites with complex microstructure*, Comp. Meth. Appl. Mech. Engng., **157**, 69–94, 1998.
14. J.C. MICHEL, H. MOULINEC, P. SUQUET, *Effective properties of composite materials with periodic microstructure: a computational approach*, Comput. Methods Appl. Mech. Engng., **172**, 109–143, 1999.
15. O. LOPEZ-PAMIES, P. PONTE–CASTAÑEDA, *Second-order estimates for the large-deformation response of particle-reinforced rubbers*, Comptes Rendus Mecanique, **331**, 1–8, 2003.
16. S. HARTMANN, P. NEFF, *Polyconvexity of generalized polynomial-type hyperelastic strain energy functions for near-incompressibility*, Int. J. Sol. Struct., **40**, 2767–2791, 2003.
17. M. BORNERT, T. BRETHERAU, P. GILORMINI, *Homogénéisation en mécanique des matériaux 2 : Comportements non linéaires et problèmes ouverts*, HERMES Science Publication, Paris 2001.
18. N. LAHELLEC, P. SUQUET, *Effective behaviour of linear viscoelastic composites: A time-integration approach*, Int. J. Sol. Struct., **44**, 2, 507–529, 2007.
19. R. BRENNER, R. MASSON, *Improved affine estimates for nonlinear viscoelastic composites*, Eur. J. Mech. A/Solids, **24**, 1002–1015, 2005.
20. H. TRUMEL, A. DRAGON, A. FANGET, P. LAMBERT, *A constitutive model for the dynamic and high pressure behaviour of a propellant-like material - Part I: Experimental background and general structure of the model*, Int. J. Numer. Anal. Methods Geomech., **25**, 551–579, 2001.
21. H. TRUMEL, A. DRAGON, A. FANGET, P. LAMBERT, *A constitutive model for the dynamic and high pressure behaviour of a propellant-like material - Part II: Model development and applications*, Int. J. Numer. Anal. Methods Geomech., **25**, 581–603, 2001.

22. S. REESE, S. GOVINDJEE, *A presentation and comparison of two large deformation viscoelasticity models*, ASME J. Enging. Mat. Tech., **119**, 251–255, 1997.
23. P. HEULLET, L. DUGAUTIER, *Modélisation du comportement hyperélastique des élastomères compacts*, Appolor et INPL, Nancy 1997.
24. A. REKIK, M. BORNERT, F. AUSLENDER, A. ZAOUI, *A methodology for an accurate evaluation of the linearization procedures in nonlinear mean field homogenization*, Comptes Rendus Mecanique, **333**, 11, 789–795, 2005.
25. P. PONTE-CASTAÑEDA and E. TIBERIO, *A second-order homogenization method in finite elasticity and applications to black-filled elastomers*, J. Mech. Phys. Solids, **48**, 1389–1411, 2000.

Received December 29, 2006; revised version July 19, 2007.
